Simultaneous UV and X-ray observations of rapidly rotating stars with AstroSat

Utkarsh Pathak
Roll No: MS16048

A dissertation submitted for the partial fulfilment
of BS-MS dual degree in Science

Under the guidance of
Prof. Kulinder Pal Singh

May 2021

Indian Institute of Science Education and Research Mohali

Sector - 81, SAS Nagar, Mohali 140306, Punjab, India

Certificate of Examination

This is to certify that the dissertation titled **"Simultaneous UV and X-ray observations of rapidly rotating stars with AstroSat"** submitted by **Utkarsh Pathak** (Reg. No. MS6048) for the partial fulfillment of BS-MS dual degree programme of the Institute, has been examined by the thesis committee duly appointed by the Institute. The committee finds the work done by the candidate satisfactory and recommends that the report be accepted.

Dr. Kinjalk Lochan   Dr. Harvinder K. Jassal   Prof. Jasjeet S. Bagla

Prof Kulinder Pal Singh

(Supervisor)

Dated: 27.05.2021

MS Thesis submission for MS16048

Utkarsh Pathak 📎 May 28

Dear sir/madam, I request you to review and approve my MS Thesis attached herewith. PS:

2

Prof.Jasjeet Singh Ba... 11:11 AM

to me ⌄
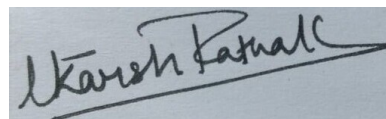
Approved,
Jasjeet

Show quoted text

--
Jasjeet Singh Bagla
Department of Physical Sciences
Indian Institute of Science Education and Research (IISER) Mohali
Knowledge City, Sector 81
Sahibzada Ajit Singh Nagar
Punjab 140306
India
https://web.iisermohali.ac.in/Faculty/jasjeet/

Declaration

The work presented in this dissertation has been carried out by me under the guidance of Prof. Kulinder Pal Singh at the Indian Institute of Science Education and Research Mohali.

This work has not been submitted in part or in full for a degree, a diploma, or a fellowship to any other university or institute. Whenever contributions of others are involved, every effort is made to indicate this clearly, with due acknowledgement of collaborative research and discussions. This thesis is a bonafide record of original work done by me and all sources listed within have been detailed in the bibliography.

Utkarsh Pathak

(Candidate)

Dated: May 27, 2021

In my capacity as the supervisor of the candidate's project work, I certify that the above statements by the candidate are true to the best of my knowledge.
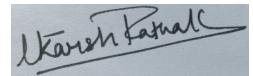
Prof. Kulinder Pal Singh

(Supervisor)

Acknowledgement

List of Figures

List of Tables

Contents

Abstract

Late type dwarf stars of spectral type K and M are among the most active stars. These stars are driven by convection and have rotating dynamo, generating the magnetic field. Stellar activity in such stars depends upon age of stars, rotation, spectral type. These stars often show energetic activities like flaring, where magnetic field lines reconnects, releasing non thermal emission by bremsstrahlung radiation (in Hard X-ray band) followed by chromospheric heating and Soft X-ray and UV radiation on cooling.

AstroSat Observations and analyses of five such rapidly rotating stars are presented here. These are: AB Dor, BO Mic, DG CVn, GJ 3331, and V405 And with a rotation period below 12 hours. Level 2 data from Soft X-ray Telescope (SXT) and UV Imaging Telescope (UVIT) onboard *AstroSat* are used for extracting UV & X-ray light curves, and X-ray images for all the sources, with X-ray spectra for BO Mic. We observed change in temperature, coronal density, and metallicity during flare and defined two states of BO Mic, quiescent and flaring state.

Spectral analysis study can be further detailed by using atomic plasma code models with variable abundances and extending the study to other sources. Mechanism behind the coronal and chromospheric activity can also be disscussed by verifying Neupert effect through UV & X-ray light curves correlation.

Chapter 1

Introduction

Late spectral type main sequence stars such as F, G, K, and M have less surface temperature thus 'cooler' as compared to O, B, A stars. These stars are mainly driven by convection and have active magnetic fields. Such stars often have rotating dynamo generating the magnetic field. These stars show energetic phenomenon and have outer convective layer which gives dynamic magnetic fields. These field lines trap ionised particles thus sustaining an outer stellar atmosphere called corona. The temperature of corona for late spectral type is of order 10 MK where as the surface temperature for M stars for eg. is 3500K. Stellar activity depends upon magnetic field which is affected by (1) age of stars: stars slows down due to magnetic stripping with time, (2) rotation: rapidly rotating stars have dynamo generated magnetic fields , (3) spectral type of stars: late spectral stars have larger convection zone. To measure activity in such a star we use indicator such as $\dfrac{L_x}{L_{bol}}$ where the ratio increases as we move from F to M. We also define Rossby number $R_0 = \dfrac{P_{rot}}{\tau_c}$, where P_{rot} is rotation period and τ_c is the convective overturn time, the time taken by the convective cell in the star to rise up [Stepien, 1994]. The young active fast rotating stars with large τ_c have a very small Rossby number ([Singh et al., 1999]).

Out of all energetic activities observed in K, M stars, flares are most common. During flare we observe an increase in temperature and X-ray luminosity. A flare occurs when magnetic field lines above star spots reconnects, releasing non thermal electrons along field lines to invade the chromosphere, where electrons collide with ions in plasma and gives out bremsstrahlung radiation (in hard x-ray band). The chromospheric plasma heats up, expands and flows up to corona where it emits soft x-ray and UV radiation on cooling by atomic recombination.

X-ray and UV are the optimal energy range for observing the hot corona and chromosphere. Such observations are made from space due to Eath's atmosphere. *AstroSat* is such a satellite launched by ISRO on 28 September 2015 at 10:00 IST. It is in 650 km circular orbit above Earth at a 6° inclination with a 98 minutes orbital period ([Singh et. al., 2017]). It has 6 different payloads on-board which are: Large Area Xenon Proportional Counter (LAXPC), a Soft X-ray Telescope (SXT), two UV Imaging Telescopes (UVIT), a Cadmium-Zinc Telluride Imager (CZTI), a Scanning Sky Monitor (SSM), and a Charged Particle Monitor (CPM). SXT and UVIT can provide simultaneous observations in UV and X-ray for fast rotators. A subset of 5 Stars have been observed here which are K, M spectral type main sequence fast rotators, with a rotation period less than half a day. The target stars studied here are AB Dor, BO Mic, DG CVn, GJ 3331, and V405 And. With these observations we attempt to understand the relation between the chromospheric and coronal activities by observing change in coronal density and metallicity during flare and define two states of BO Mic, quiescent and flaring state.

In §2 and §3, I have described the instrumentation, the target stars, the observation and the data details. UVIT and SXT analysis is described in §4 and §5 respectively. A conclusion on the results is found in §6, and the future plans follows in §7.

Chapter 2

Instrumentation

2.1 Ultra-Violet Imaging Telescope (UVIT)

Ultra Violet Imaging Telescope is a twin Ritchey Chretien telescope with three different channels: Far UV (130 nm – 180 nm), Near UV (200 nm – 300 nm), and VIS (320 nm – 550 nm). It has a total focal length of 4750 mm with a Field of View of 28 arc-min and has hyperbolic primary & secondary mirrors of 140 mm optical diameter. It has fast optics f/4.5 and has a diameter of 380 mm (optical diameter $\sim$ 375 mm). The three main contributors to the PSF are optics, detector, and drift of the aspect. The largest contribution is from 1 arc-seconds FWHM. Both UV channels have a spatial resolution (FWHM) of less than 1.5 arc-seconds, while the VIS channel has a spatial resolution of 2.5 arc-seconds [Tandon et al., 2020]. It has a pixel scale of 3.33 arc-seconds / pixels, i.e. 0.416 arc – seconds / sub-pixel. UVIT has a temporal resolution of 2 ms. FUV and NUV channels have 6 filters each, while the VIS channel has 5 filters. The filters used during the observation from the FUV channel are CAF2-1 (called F148W where 148.1 ± 50 nm is the mean wavelength of the band) and Silica-1 (N242W having a 241.8 ± 78.5 nm mean wavelength), NUVN2 (N279N having a 279.2 ± 9.0 nm mean wavelength) for the NUV channel. The mean effective area of the telescopes, for each channel, is 10 cm^2 for the FUV, 40 cm^2 for NUV and 50 cm^2 for the VIS channel. Detectors used are intensified CMOS type (Complementary Metal Oxide Semiconductor) with an aperture of 39 mm diameter, which can either be operated in photon counting mode or integration mode. It has an entire array of 512 X 512 pixels which can capture the entire field at a frame rate of 29 frames/s or part of the field in window mode at frame rates up to 600 frames s^{-1} [Tandon et al., 2020].

3

2.2 Soft X-Ray Telescope (SXT)

Soft X-ray telescope captures efficient response for soft x-rays from (0.3 − 8.0) keV. It consists of a mirror assembly with a focal plane camera assembly (FPCA) housing a cool charged coupled device (CCD-22) with a cover at the top end of the telescope at angle of 256 degrees. It has 40 set of coaxial and con-focal shells of conical mirrors approximated to parabolical and hyperboloidal shapes arranged in Wolter I optics, nested together to improve the effective area to 90cm^2 at 1.5 keV [Singh et al., 2014]. It has a total focal length of 2 meters with a PSF of 2 arc-min (FWHM) and an HPD of 10 arc-min. The CCD – 22 used is a MOS device made by E2V Technology Inc., with a 3 phase transfer with an open electrode structure of bandpass of 0.2 to 10 keV. It has an operating area of 610 X 602 array and a 600 X 602 array storage region, giving a 600 x 600 good image area. Each pixel has 40μm x 40μm dimension, and the field has a pixel scale of 4.12 arc-seconds per pixel, thus a field of view of 40 arc-min [Singh et. al., 2017]. There are four individual ^{55}Fe radioactive calibration sources for in-flight calibration placed at the corner of the CCD and observed at 5.9 keV, 6.5 keV. There are six modes of observation:

- Photon Counting (PC) where energy tagged events from the whole field are collected for above threshold energy (100-200 eV by default) with a time resolution of 2.375 seconds.

- Photon Counting Window (PCW), which is PC with a user-defined window.

- Fast Windowed Photon Counting (FW), which has fixed 150 x 150 pixel centered window with a resolution time of 278 ms.

- Bias Map (BM), which is measured for whole CCD without any threshold.

- House-Keeping (HK), which records health parameters of the electronic system and records when there is a failure of both LBT channels (main & redundant).

- Calibration (Cal), which is used for calibrating SXT by radioactive calibration sources.

We used SXT data that was obtained using the PC mode. We used low energy threshold of 0.3 keV and high energy threshold of 7.0 keV for X-ray events in our analysis.

2.3 Galaxy Evolution Explorer (GALEX)

Galaxy Evolution Explorer (GALEX) is a NASA explorer mission launched on an Orbital Sciences Corporation Pegasus rocket on 2003 April 28 at 12:00 UTC into a circular orbit above Earth at 700 km and $29°$ inclination [Morrissey, 2005]. It has performed all sky survey in two UV bands, FUV (134 nm - 179 nm) and NUV (177 nm - 283 nm). It was operational till 2012 February 7 and decommissioned 2013 June 28.

It is a f/6 Ritchey Chretian telescope with a 50 cm primary diameter and a focal length of 299.8 cm. It has two photon counting micro channel-plate (MCP) to image sky simultaneously in NUV and FUV. The peak effective area for the telescope, for each channel is, 36.8 cm^2 at 148 nm for FUV and 61.7 cm^2 at 220 nm for NUV. The Field of view for FUV band is $1.27°$ and for NUV band is $1.25°$. It has a pixel scale of 1.5 arc-seconds per pixel and an image resolution of 4.2 arc-seconds for FUV band and 5.3 arc-seconds for NUV band [Morrissey, 2007]. I have used GALEX GRelease ops-v7 AIS imaging survey data for comparing different stellar fields and matching stellar patterns to reduce astrometric error in UVIT L2 data.

Chapter 3

Observations and Data details

3.1 Stars Samples and their Properties

- AB Dor is an ultrafast rotator with a rotational speed and rotational period of 90 km/s and 0.514 days respectively ([Kürster, 1994]). It is a young active dwarf star about $40 - 50$ Myrs old ([Guirado et al., 2011]) which is also the constituent member of the AB Doradus Moving Group. It is a quadruple system of a pair of binary system AB Dor A, AB Dor B, where AB Dor B is 60 times bolometrically fainter than AB Dor A. AB Dor A companion AB Dor C has a 0.16 arc-seconds separation, which is unresolvable in UVIT images. AB Dor B constituents AB Dor Ba and AB Dor Bb were observed with Australian Telescope Compact Array with a 0.7 arc-seconds separation at radio wavelength. AB Dor shows high level of magnetic activity with an average $\log\left(\dfrac{L_x}{L_{bol}}\right) = -3$. AB Dor is also a calibration source for reflection grating spectrometer onboard XMM-Newton.

- BO Mic is an active K3V(e) star present in the constellation Microscopium, about 51.02 ± 1.5 parsecs away ([Gaia Collaboration and Brown et al., 020b]). It was first reported in the all-sky EUV ROSAT mission, with the largest stellar flare. It has a radial velocity of 6.5 ± 2.0 km/s with an estimated $v\sin i$ of 120 ± 20 km/s; it is called Speedy Mic for its fast rotation [Bromage et al., 1992] with a rotation period of 0.380 $\pm$ 0.004 days [Cutispoto et al., 1997]. It is possibly a young PMS for its high lithium abundance, strong photometric, and chromospheric activity [Anders et al., 1993]. It has two states: the quiescence state and the flaring state. It has been observed to have an average X-ray flux of 3.7 x 10^{-12} ergs cm^{-2} s^{-1} for quiescence state and 7.9 x

10^{-12} ergs cm^{-2} s^{-1} for the flaring state [Singh et al., 1999]. Its differential rotation is weaker than the sun, with its spot pattern changing nearly every 2.5 stellar rotations [Wolter, U. et al., 2005].

- DG CVn is a binary M dwarf system with a 0.2 arc-seconds separation between the components, with one of them being a fast rotator. It is 18.29 ± 0.11 parsecs away [Gaia Collaboration and Brown et al., 2018] and about 30 Myrs old. It is a fast rotating star with rotation speed of 50 km/s and a rotation period of 0.28 days [Mohanty and Basri, 2003]. DG CVn is listed in Washington Double Star Catalog and ROSAT All-Sky Survey Bright Source Catalog with $L_X \sim 2.0 \times 10^{28}$ erg s^{-1} and $\frac{L_X}{L_{bol}} \sim -3.22$. Ca H & K lines in emission have been observed [Beers et al., 1994]. It has been observed by the Burst Alert Telescope (BAT) on board the Swift satellite, with a peak 15-50 keV flux of 300 mCrab [Osten et al., 2016].

- GJ 3331 (BD 211074) It is a tertiary M star system listed in Washington Catalog of Visiual Double Stars [Mason et al., 2001] and Wide Field Camera (WFC) Bright Source Catalog as RE 0506-213 [Pounds et al., 1993]. The primary component is GJ3331, an M1.5 star with V = 10.29 mag, the secondary component GJ3332, is an M2.5 star with V = 11.67 mag. The tertiary component BD 211074C is an M5 star [Jao et al., 2003]. GJ 3331 is a fast rotator with a rotation period of 0.34 days. It is acitve in EUV, EUVE, and X-ray with a strong X-ray emission detected by *ROSAT* i.e. $L_X \sim 1.4 \times 10^{29}$ erg s^{-1} and $\frac{L_X}{L_{bol}} \sim -3.01$, [Voges et al., 1999]. Components A and B are resolvable in UVIT images, however component BC remains unresolvable.

- V405 And: It an X-ray bright source listed in RASS (RX J0222.4+4729) [Voges et al., 1996]), which is a RS CVn binary system with period of 0.46 days. Both components are fully convective with a mass of 0.42 M$_\odot$ for primary and 0.21 M$_\odot$ for secondary component. The components have M0V and M5V spectral types, with both showing strong Hα emission lines [Chevalier and Ilovaisky, 1997]. A detailed photometric study have been carried out to produce light curves in various optical bands [Vida et al., 2009].

Important properties of stars have been listed in Table 3.1.

Table 3.1: Properties of stars observed with *AstroSat*

	AB Dor	BO Mic	DG CVn	GJ 3331	V405 And
Basic Parameters					
Spectral type	K0V	K3V	M4Ve	M2 D	M0 D
V (mag)	7.0	9.34	12.02	10.41	11.57
Distance* (pc)	14.85 ± 0.10	51.02 ± 1.50	18.29 ± 0.11	19.83 ± 0.01	42.11 ± 0.12
P_{rot} (d)	0.514	0.380	0.2683	0.34	0.46

*Distances are based on parallax measurements in Gaia EDR3

[Gaia Collaboration and Prusti et al., 2016, Gaia Collaboration and Brown et al., 020b].

DG CVn distance is calculated from parallax measurement in Gaia DR2

[Gaia Collaboration and Prusti et al., 2016, Gaia Collaboration and Brown et al., 2018].

3.2 Observation Log and Data description

3.2.1 AstroSat Observation Log

Table 3.2: Log of AstroSat Observations

Star Name	Instrument	Observation ID	Start Time (UT) Y:M:D:H:M:S	Stop Time (UT) Y:M:D:H:M:S	Effective Exposure (s)	Mean Count Rate SXT; NUV/FUV 0.3-7.0 keV; F3/F5
AB Dor	SXT	9000000274	2016:01:15:11:57:43	2016:01:16:04:46:40	17346	1.075±0.009
AB Dor	SXT	9000000306	2016:01:31:11:13:32	2016:02:01:05:11:32	17272	1.132±0.009
BO Mic	SXT	9000002104	2018:05:17:21:24:36	2018:05:20:12:34:13	41862	0.173±0.003
	UVIT FUV F148W	9000002104	2018:05:17:22:42:12	2018:05:19:18:48:02	17138	0.73±0.12
DG CVn	SXT	9000001218	2017:05:11:07:47:57	2017:05:12:03:33:19	21687	0.065±0.002
	UVIT NUV N242W	9000001218	2017:05:11:09:39:19	2017:05:12:03:10:48	81	9.39±3.12
	UVIT FUV F148W	9000001218	2017:05:11:09:39:14	2017:05:12:03:10:44	1102	0.40±0.16
GJ 3331	SXT	9000000898	2016:12:18:13:56:41	2016:12:19:06:36:30	14748	0.200±0.004
	UVIT NUV N279N	9000000898	2016:12:18:13:58:45	2016:12:19:09:59:29	15760	2.40±0.40
	UVIT FUV F148W	9000000898	2016:12:18:13:58:49	2016:12:19:09:59:25	11749	0.32±0.12
V405 And	SXT	9000000638	2016:09:01:00:50:55	2016:09:03:02:09:38	46927	0.052±0.001

3.2.2 UVIT Data structure

The UVIT L2 data is processed through UVIT pipeline v6.3 and onwards (DG CVn data processed using UVIT pipeline v4.5). For a single observation, the L2 data is stored in folders, orbit-wise. Each folder uvt_N, where N is the orbit number, has the following files in it:

- *A_l2img.fits: Image file in astronomical coordinates, used for identifying star orbit-wise.

- *I_l2img.fits: Image file in instrument coordinates, used to obtain instrument coordinates of star.

- *A_l2exp.fits: Exposure map for image file in astronomical coordinates.

- *A_l2err.fits: Error map for image file in astronomical coordinates.

- *l2ce.fits: Corrected events list, used for making light curves.

- *l2dr.fits: The Relative Aspect Series (RAS) file.

The astrometric corrections are done on *imb.fits, combined orbits image file present in the folder uvit_ci, by comparing with fd or nd-int.fits GALEX AIS image file for each observation.

3.2.3 SXT Data structure

The SXT Level 2 data, provided by ISSDC, is produced through sxtpipeline v 1.4b. Each SXT observation have multiple orbit-wise folders. Cleaned event files of the individual orbit (*sxtPC00_level2_cl.evt) are used in analysis. To avoid the time-overlaps in the events from consecutive orbits, all level2 cleaned events are merged using Julia 1.0.2 based merger tool "SXTTools" provided by SXT POC team.

Chapter 4

UVIT Analysis

UVIT data for BO Mic, DG CVn, and GJ3331 was analyzed.

4.1 Star Identification & Astrometry

The target star location in the UVIT L2 data was found by matching stellar patterns between the combined orbits image file and the GALEX image file from GRelease ops-v7_0_5 (v7_0_3 for GJ3331) AIS imaging survey data for the same channel (FUV, NUV). The as-

Table 4.1: Log of GALEX observations used for Astrometric correction

Star Name	Band	Observation ID	Exposure (seconds)	Filename
BO Mic	Band 2 (FUV, 153.9 nm)	6384391446235975918	189.05	AIS_383_sg71-fd-int.fits
DG CVn	Band 2 (FUV, 153.9 nm)	6379324891286471537	145.15	AIS_239_sg66-fd-int.fits
DG CVn	Band 1 (NUV, 226.7 nm)	6379324891286471537	145.15	AIS_239_sg66-nd-int.fits
GJ 3331	Band 2 (FUV, 153.9 nm)	6381435928915739603	176.00	AIS_299_sg43-fd-int.fits
GJ 3331	Band 1 (NUV, 226.7 nm)	6381435928915739603	176.00	AIS_299_sg43-nd-int.fits

trometric error was calculated by comparing coordinates of common sources with GALEX catalog for each image field. 5 common sources with GALEX-FUV were used for matching stellar pattern in BO Mic UVIT F148W field. 9, 6 common sources with GALEX-FUV, GALEX-NUV were used for matching stellar pattern in DG CVn UVIT F148W, and UVIT N242W field respectively. 8, 6 common sources with GALEX-FUV, GALEX-NUV were used for matching stellar pattern in GJ 3331 UVIT F148W, and UVIT N279N field respectively. The astrometric corrections were done by translating and rotating coordinates through astropy version 4.0.1. The astrometric calibrations were also verified with the SIMBAD catalog. The astrometric error before and after corrections for each field is given in

table 4.2. The astrometric error for GJ 3331 UVIT N279N field was negligible, however it was an order of degree for GJ 3331 UVIT F148W. The field was was matched with its NUV counterpart and the coordinates were translated.

Table 4.2: Astrometric Error for each field before (& after) astrometric corrections

Star Name	Instrument	Observation ID	Error with GALEX	Error with SIMBAD
BO Mic	UVIT FUV F148W	9000002104	7.7" (7.7")	8" (8")
DG CVn	UVIT FUV F148W	9000001218	15.68' (8")	15.65' (11")
DG CVn	UVIT NUV N242W	9000001218	13.14' (7.5")	13.13' (16")
GJ 3331	UVIT FUV F148W	9000000898	57.84' (13")	57.89' (16")
GJ 3331	UVIT NUV N279N	9000000898	0" (0")	0" (0")

4.2 Orbit wise transformation from Astronomical Coordinates to Instrument Coordinates

The target star was found in orbit-wise image file with astronomical coordinates, *A_l2img.fits, by matching stellar pattern with combined orbits image file *imb.fits. The coordinate system was transformed to instrument coordinates by rotation and flip, given in table 4.3. The modified image file was compared to orbit-wise image file with instrument coordinates, *I_l2img.fits. Instrument coordinates of target star were used further in source extraction.

Table 4.3: Transformation of *A_l2img.fits to *I_l2img.fits

Star Name	Instrument	Observation ID	Rotation '+' Anticlockwise	Flip	Error (sub-pixels)
BO Mic	UVIT FUV F148W	9000002104	-79.28°	No	0.5
DG CVn	UVIT FUV F148W	9000001218	+94.06°	Yes	0.7
DG CVn	UVIT NUV N242W	9000001218	+151.01°	No	3.2
GJ 3331	UVIT FUV F148W	9000000898	+62.82°, +64.41°	Yes	0.8
GJ 3331	UVIT NUV N279N	9000000898	-72.47°, -71.12°	No	0.7

4.3 Source Extraction & Light curve

After finding the instrumental coordinates of target star for each orbit, the source and the background radius were set. *Curvit* python script was used for extracting light curves orbit-wise through 'curve' function. The script is developed by P.Joseph from IIA.

5 Different radii (3.33, 6.24, 12.48, 20.8, 39.52) arc-seconds, centered at the star of interest, were compared to fix the source radius. The point spread function (PSF) for UVIT filters can be divided into two parts: narrow core and the extended pedestal. The extended pedestal is mainly caused by scattering of photons on mirror surface and supporting ribs. The FUV filter F148W was found to be extended to 3.33 arc-seconds ([Tandon et al., 2020]). This gave the minimum allowed source radius of 3.33 arc-seconds. Light curves for each orbit were made to observe the variation in countrate for different source radii. Source region were checked to ensure no contribution from other independent photon events.

Background region were selected within 1 arc-minute of source region by comparing estimated countrate. 5 different radii (6.66, 12.48, 24.96, 41.6, 79.04) arc-seconds were compared to fix the background radius. Background radii was kept twice of the source radii for most of the observations. The error in countrate is calculated using poisson distribution for photon events.

The time bin width was selected from (1, 5, 10, 20, 50) seconds. The UVIT L2 data is sparse and scattered, thus could not get to finer time resolution. Different time bin widths were compared to achieve a sufficient number of data points with small errors for each data point. The countrate was converted to Flux using Unit Conversion factor for each filter [Tandon et al., 2020]. Following are the settings for each observation:

- BO Mic had a 6.25 arc-seconds source radius, 12.5 arc-seconds background radius, and a 50 seconds wide time bin. The combined orbits UVIT-F148W light curve for BO Mic had a flare near the end of the observation.

- DG CVn had a 12.5 arc-seconds source radius, a 25.0 arc-seconds background radius, and a 15 seconds wide time bin for both F148W & N242W filters. The data for DG CVn is scattered and sparse.

- GJ 3331 had a 3.33 arc-seconds source radius due to proximity to secondary member GJ 3332, a 25.0 arc-seconds background radius, and a 20 seconds wide time bin for F148W data but 15 seconds wide time bin for N279N data.

13
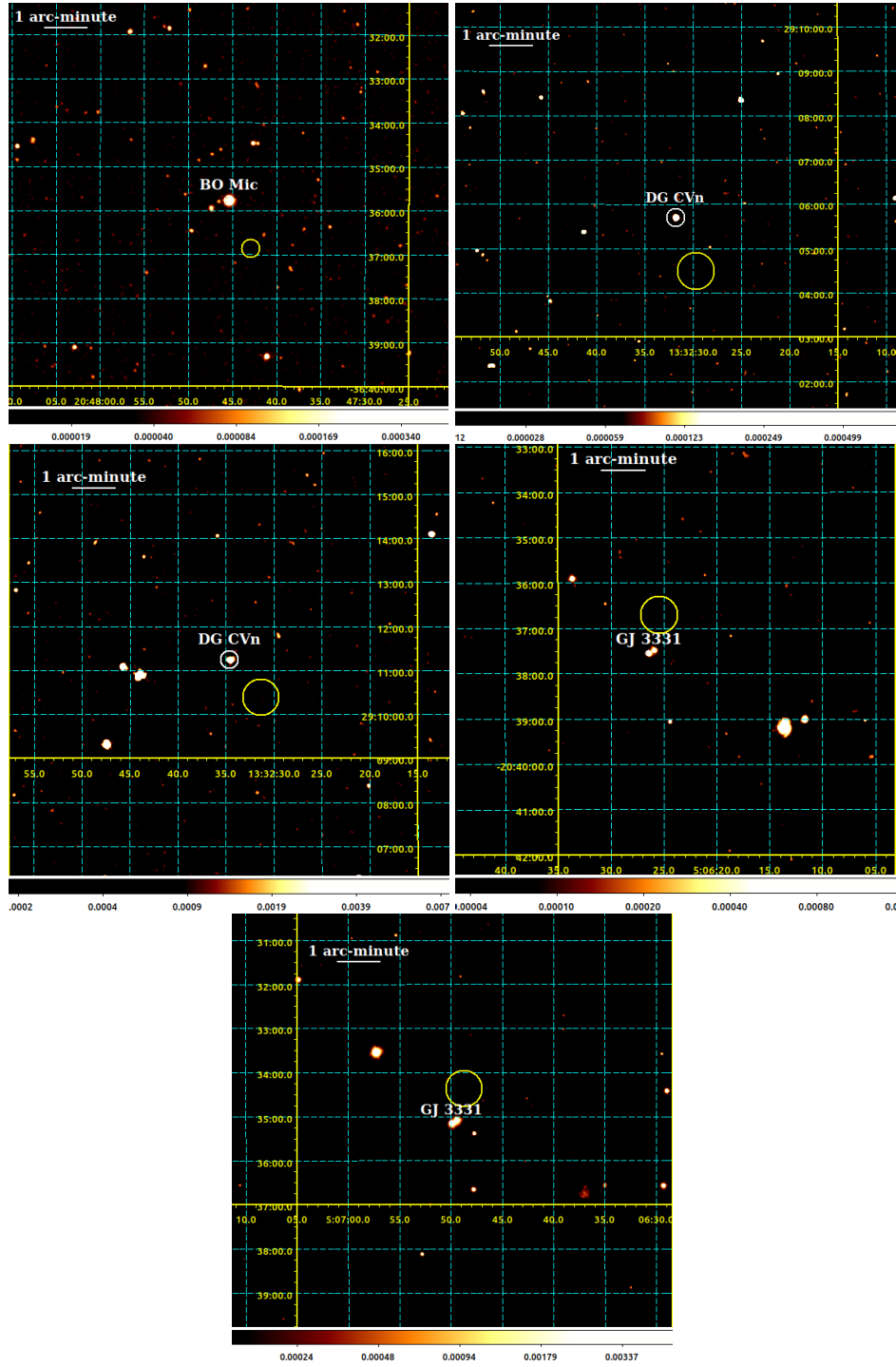
Figure 4.1: NUV and FUV images for each observation with the AsroSat UVIT (Clockwise from top left source and filter: BO Mic F148W, DG CVn F148W, GJ 3331 F148W, GJ 3331 N279N, and DG CVn N242W). The white circle shows the extraction region for the light curves and the yellow circle shows the background region.

Figure 4.2: Combined orbits light curve for each observation in UV. (Clockwise from top, source and time bin width: BO Mic F148W - 50s, DG CVn N242W - 15s, GJ 3331 N279N - 15s, GJ 3331 F148W - 20s, and DG CVn F148W - 15s).

Chapter 5

SXT Analysis

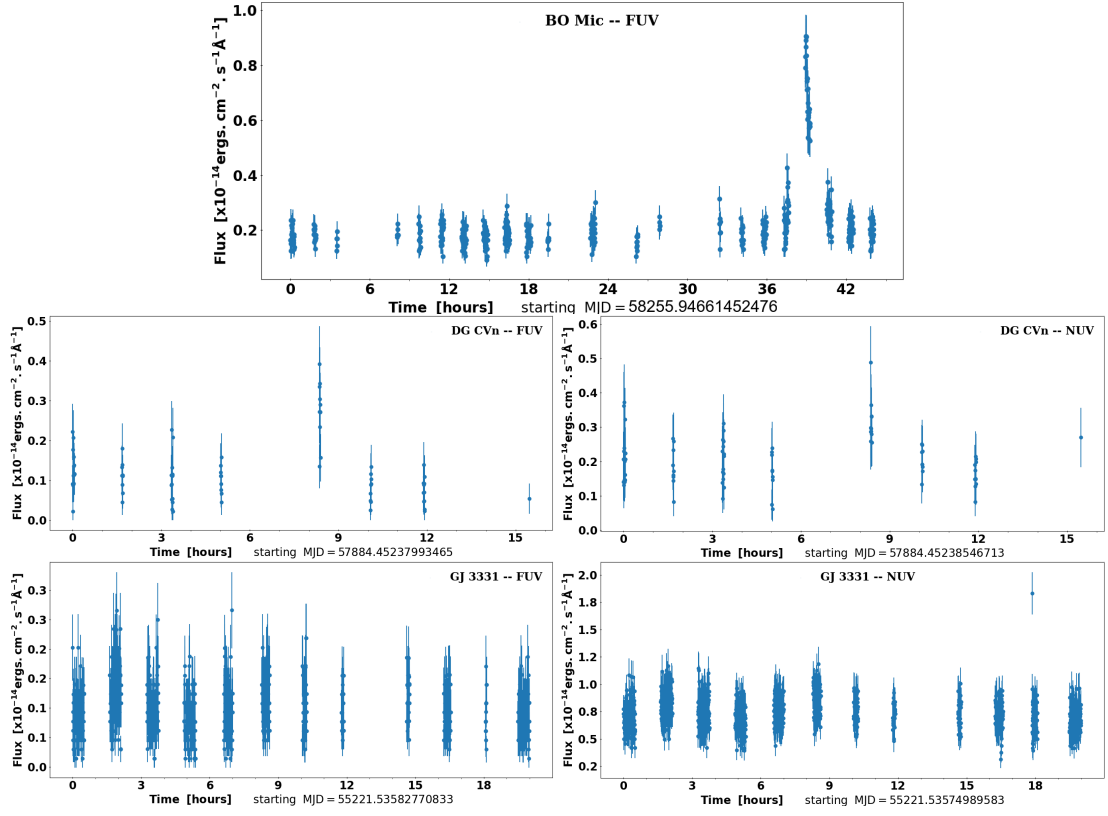SXT Level 2 Data was received from the ISSDC for each individual orbit for an observation. Th cleaned event files of the individual orbits were merged into a single cleaned event file to avoid the time-overlaps in the events from consecutive orbits using Julia based merger tool "SXTTools". SXT merged cleaned L2 events files were analysed for all the six observations. The light curves, images, and spectra were extracted using XSELECT (V4.2k) package built-in HEASoft.

5.1   Images

X-ray images were extracted by setting energy filter to (0.3-3.0) keV as the calibration sources are fainter and the target sources are brighter in this range. The source extraction radius was also set by radial profile analysis in SAO DS9. The plot between Surface Brightness and Average Radius was examined using 25 annuli, ranging from 0.5 arc-minute to 19 arc-minute placed around the target star.

The extraction radius was chosen by studying the radial profiles and thus finding the radius where the surface brightness of star levels down to the background brightness, which was latter used in making light curves and spectra. AB Dor Obs1 (id: 9000000274) and Obs2 (id: 9000000306) have an extraction radius of 16 arc-minute and are relatively bright source as shown in figure 5.1. BO Mic have a 12 arc-minute extraction radius. While DG CVn, GJ 3331, and V405 And have a 8, 10, 10 arc-minute extraction radius.

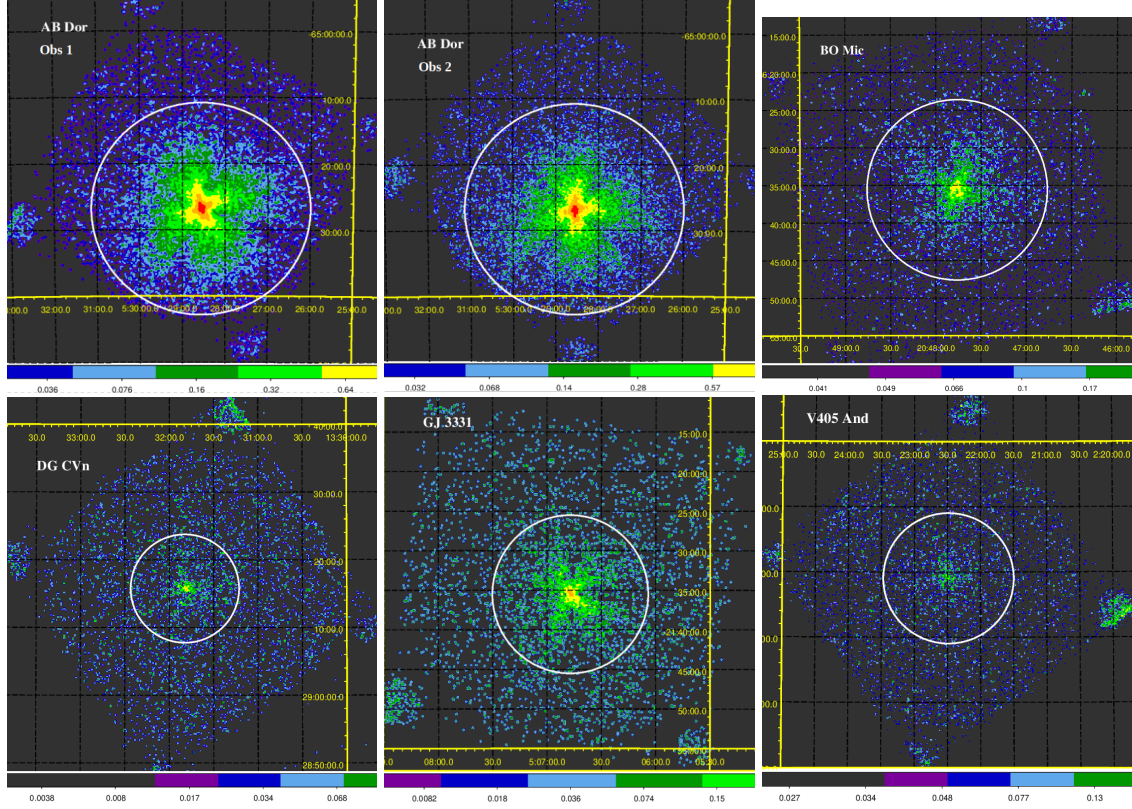Figure 5.1: X-ray images of the stars in (0.3-3.0) keV energy band observed with the AsroSat SXT (Clockwise from top left, source - extraction radius: AB Dor (Obs 1) - 16', AB Dor (Obs2) - 16', BO Mic - 12', V405 And - 10', GJ 3331 - 10' and DGCVn - 8'). The white circle shows the extraction region for the light curves and spectra and the image has been smoothed with a Gaussian function of 3 pixel radius.

5.2   X-ray Light Curves

The X-ray light curves were extracted using lcurve program from XRONOS 6.0 package built-in HEASoft. XSLECT and lcurve allowed to set the time bin width, extraction radius, and the energy range for each observation.

The complete energy range for X-ray light curve is (03.-7.0) keV, where energy below 0.3 keV was not taken as that contains thermal & electronic noises. The energy is further defined into Soft band (0.3 - 2.0) keV and Hard band (2.0 - 7.0) keV. The hardness ratio was defined as HR = H/S. The light curves were also verified for periodicity at rotational period and were folded on arbitrary epoch by efsearch and efold method respectively.

Figure 5.3 shows the folded light curves for each observation. Figure 5.2 shows the X-ray light curve in energy range (0.3 - 7.0) keV for each observation. BO Mic X-ray light curve shows a flare in the observation which was further studied in the BO Mic spectra.
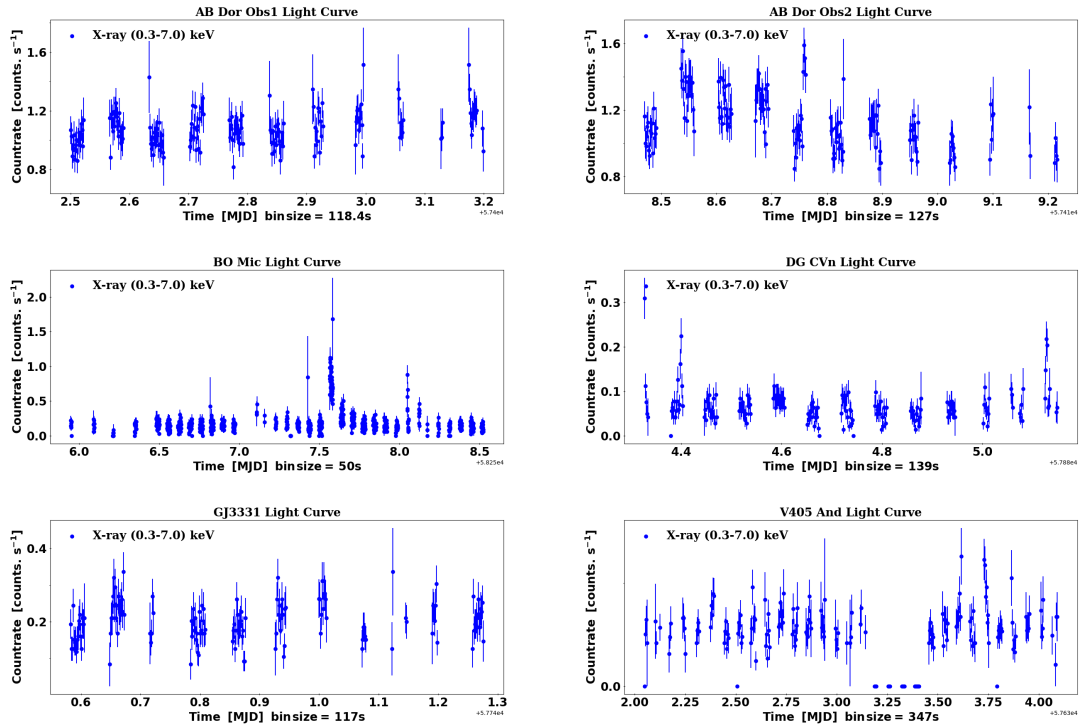

Figure 5.2: X-ray light curve in range (0.3 - 7.0) keV. (Clockwise from top left: AB Dor (Obs 1), AB Dor (Obs2), DGCVn, V405 And, GJ 3331, and BO Mic).
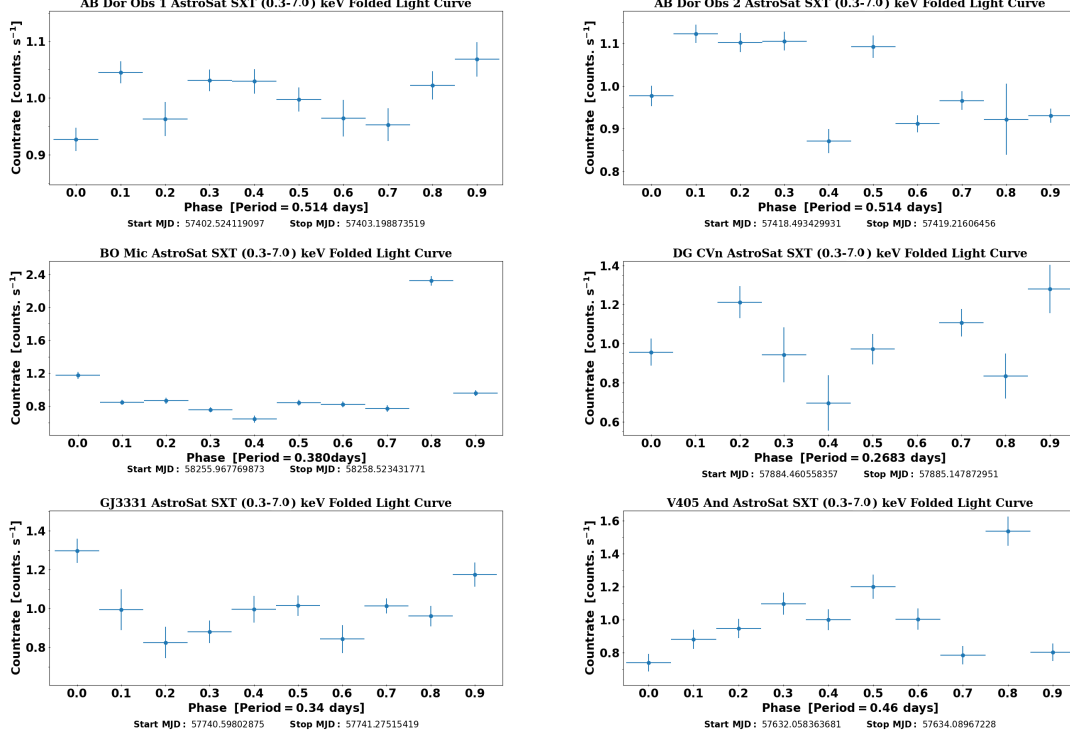
Figure 5.3: Folded X-ray light curve for each observation in (0.3-7.0) keV energy range with arbitrary epoch. (Clockwise from top left: AB Dor(Obs 1), AB Dor (Obs2), DGCVn, V405 And, GJ 3331, and BO Mic)

5.3 Spectra

The X-ray spectra for BO Mic was extracted using XSPEC 12.11.1 package built-in HEA-Soft. Good Time Intervals (GTI) were made on (0.3 - 7.0) keV light curve for dividing the whole spectra into flaring state and quiescent state, corresponding to the flare seen in BO Mic X-ray light curve. Region filter was applied for extracting the spectra.

Source spectra were grouped with background spectra, the response file, and the auxiliary response file provided by the SXT POC team. The background spectrum is subtracted from the source spectrum. The response file describes the response of the spectrum to the incident X-ray, and the auxiliary response file shows the relation between area and energy. The filenames used here are SkyBkg_comb_EL3p5_Cl_Rd16p0_v01.pha, sxt_pc_mat_g0to12.rmf, and sxt_pc_excl00_v04_20190608.arf. The spectrum was prepared while ensuring grouped channels to have counts above 25 (5 σ error). The spectrum was observed for (0.3 - 7.0) keV in both cases. The photospheric solar elemental abundance table provided by Martin Asplund [Asplund et al., 2009] was used here for setting the coronal abundance of BO Mic.

Two models were used in different arithmetic expressions to define the four different spectral models in both cases. Multiplicative model "TBABS" describes absorption due to Inter-Stellar Medium, which includes molecules, dust, and grains. It varies hydrogen column density N_H (cm^{-2}) to do spectral fitting. Additive model "APEC" where APEC stands for Astrophysical Plasma Emission Code, describes emission from collisionally ionized diffused gas in the star. It has four different parameters to set for spectral fitting:

- T (keV): The plasma temperature.

- Elemental Abundance: The coronal abundances of the elements H, He, C, N O, Ne, Mg, Al, Si, S, Ar, Ca, Fe, Ni were fixed relative to the solar photospheric abundance values as given by [Asplund et al., 2009].

- Redshift: The redshift for BO Mic is set to 0 (frozen).

- norm $= \dfrac{10^{-14}}{4\pi R^2} \int n_e n_H dV$: Here R is the distance from star (cm), n_e and n_H are electron and H densities (cm^{-3}).
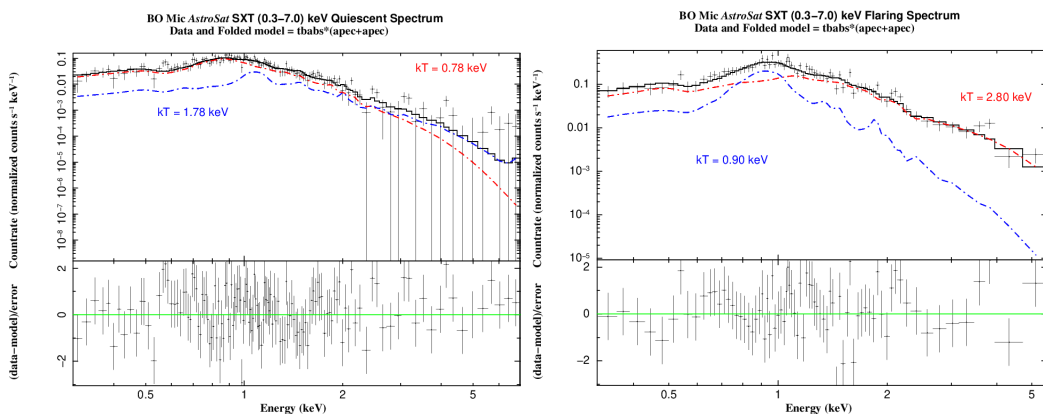

Figure 5.4: X-ray Spectra of BO Mic and best fit models as observed with *AstroSat* SXT during the quiescent state (left) and Flaring state (right).

Table 5.1: Spectral Parameters for BO Mic obtained from SXT data (0.3 - 7.0 keV) for quiescent state.

Spectral Model	Parameters								
	n_H	kT_{1apec}	Z	A_1	kT_{2apec}	A_2	χ^2_ν/dof	Flux	Luminosity
	x 10^{20} cm^{-2}	keV		x 10^{-3}	keV	x 10^{-3}		x 10^{-12} ergs cm^{-2} s^{-1}	x 10^{30} ergs s^{-1}
tbabs*apec	1.009 x 10^{-15}	1.56	1.0	2.16	-	-	3.24/134	3.06	0.95
tbabs*apec	1.009 x 10^{-15}	$0.91^{+0.052}_{-0.037}$	$0.094^{+0.027}_{-0.021}$	$5.64^{+0.55}_{-0.57}$	-	-	1.14/133	3.73	1.16
tbabs*(apec+apec)	1.4 x 10^{-17}	1.56	1.0	1.08	1.56	1.08	3.29/132	3.06	0.95
tbabs*(apec+apec)	$3.82^{+4.6}_{-3.8}$	$0.78^{+0.060}_{-0.070}$	$0.102^{+0.096}_{-0.049}$	$4.95^{+2.53}_{-2.15}$	$1.78^{+0.89}_{-0.48}$	$0.71^{+0.44}_{-0.43}$	0.97/131	3.62	1.12

Table 5.2: Spectral Parameters for BO Mic obtained from SXT data (0.3 - 7.0 keV) for flaring state.

Spectral Model	Parameters								
	n_H	kT_{1apec}	Z	A_1	kT_{2apec}	A_2	χ^2_ν/dof	Flux	Luminosity
	x 10^{20} cm^{-2}	keV		x 10^{-3}	keV	x 10^{-3}		x 10^{-12} ergs cm^{-2} s^{-1}	x 10^{30} ergs s^{-1}
tbabs*apec	2.96 x 10^{-11}	2.76	1.0	11.14	-	-	3.12/74	15.53	4.82
tbabs*apec	$10.58^{+4.18}_{-3.30}$	$1.089^{+0.104}_{-0.099}$	$0.053^{+0.027}_{-0.021}$	$27.26^{+4.73}_{-3.56}$	-	-	1.66/73	12.39	3.85
tbabs*(apec+apec)	1.52 x10^{-10}	2.75	1.0	5.57	2.75	5.57	3.21/72	15.52	4.82
tbabs*(apec+apec)	$2.20^{+3.93}_{-2.20}$	$2.80^{+1.20}_{-0.73}$	$0.15^{+0.50}_{-0.15}$	$11.43^{+3.07}_{-2.54}$	$0.90^{+0.08}_{-0.07}$	$1.68^{+0.35}_{-0.33}$	1.18/71	15.25	4.73

Single temperature model with solar abundances in both cases were found to be statistically unacceptable ($\chi^2_\nu \sim 3.24$ for quiescent state and 3.12 for flaring state). Two temperature model with solar abundance also had a high χ^2_ν for both case (3.29 for quiescent state and 3.21 for flaring state).

For quiescent state, two temperature model with non-solar abundance have $\chi^2_\nu \sim 0.97$ with a flux of 3.62 x 10^{-12} ergs cm^{-2} s^{-1}. It has a hotter component of 1.78 keV and a cooler component of 0.78 keV, and it has a sub-solar metal abundance of 0.102. The emission measure for high-Temperature component is 15.41 x 10^{52} cm^{-3} and for low temperature is 2.21 x 10^{52} cm^{-3}. The electron density was calculated by using corotation radius R_* = 1.06 $R_\odot$. Electron density for high-Temperature component is 9.57 x 10^9 cm^{-3} and for low-Temperature is 3.62 x 10^9 cm^{-3}.

For flaring state, two temperature model with non-solar abundance have $\chi^2_\nu \sim 1.18$ with a flux of 15.25 x 10^{-12} ergs cm^{-2} s^{-1}. It has a hotter component of 2.8 keV and cooler component of 0.9 keV, and it has a sub-solar metal abundance of 0.15. The emission measure for low-Temperature component is 5.23 x 10^{52} cm^{-3} and for high temperature is 35.60 x 10^{52} cm^{-3}. Electron density for low-Temperature component is 5.57 x 10^9 cm^{-3} and for high temperature is 14.54 x 10^9 cm^{-3}.

Chapter 6

Conclusion

Astrometric corrections were done on UVIT image fields, with astrometric error calculated from SIMBAD as: BO Mic (F148W, 8"); DG CVn (F148W, 11"; N242W, 6"); GJ 3331 (F148W, 16"; N279N, 0").

We developed an understanding of different parameters and their role in extracting a successful light curve and spectra: time bin width, source radius, and background radius, time filters, energy filters. Light curves for combined orbits have been extracted for AB Dor Obs 1 & 2 (X-ray), BO Mic (F148W & X-ray), DG CVn (F148W & N242W & X-ray), GJ 3331 (F148W & N279N & X-ray), V405 And (X-ray). A flare has been observed for BO Mic in F148W & X-ray 0.3-7.0 keV light curve.

We studied BO Mic spectra and observed an increase in X-ray flux (for 0.3 - 7.0 keV) from 3.62 x 10^{-12} ergs cm^{-2} s^{-1} to 15.25 x 10^{-12} ergs cm^{-2} s^{-1} during flaring state compared to quiescent state. It was also accompanied with increase in the the temperature from 1.78 keV to 2.80 keV, an increase in the emission measure from 2.21 x 10^{52} cm^{-3} to 35.60 x 10^{52} cm^{-3}, and increase in electron density from 3.62 x 10^9 cm^{-3} to 14.54 x 10^9 cm^{-3} of the hot component during flare as compared to the quiescent state.

The flux and abundance value for quiescent state ((3.62 x 10^{-12} ergs cm^{-2} s^{-1}, 0.102) were comparable to the reported quiescent state values (3.7 x 10^{-12} ergs cm^{-2} s^{-1}, 0.18) for BO Mic by [Singh et al., 1999]. The flare observed here is brighter than the previous flare as shown by an increase in flux (by order of ~ 1.93) and decrease in the coronal abundance (by order of ~ 0.65) from the reported values of flaring state by [Singh et al., 1999]. There was also an increase in emission measure by order of ~ 2.5, 3.0 for hot component in quiescent and flaring state from pervious reported values in [Singh et al., 1999].

Chapter 7

Future Plan

Neupert effect discovered in 1968, is an empirical result stating that the time integral of Hard X-ray light curve is correlated with Soft X-ray light curve. This can be traced back to energetic electrons being responsible for Hard X-ray emission by collisional bremsstrahlung also acting as the main source of chromospheric heating and chromospheric evaporation, leading to Soft X-ray & UV emission on cooling by atomic recombination. This empirical result can be verified by correlating the observed flare in BO Mic UV and X-ray light curve and definig time lags.

BO Mic spectral analysis can be extended further by using atomic plasma code models with variable abundances, where we can fit individual elemental abundance by using estimated coronal or photospheric abundance from the literature. Doing a detailed flare study by analysing higher time resolution data from SXT and UVIT around the flare.

The spectral analysis will be extended to other sources to measure the plasma temperature, emission measure and the coronal abundances of all sources, comparing the properties with the Sun.

Bibliography

[Anders et al., 1993] Anders, G. J., Jeffries, R. D., Kellett, B. J., and Coates, D. W. (1993). Speedy Mic: a very young, rapidly rotating K star. *Monthly Notices of the Royal Astronomical Society*, 265(4):941–945.

[Asplund et al., 2009] Asplund, M., Grevesse, N., Sauval, A. J., and Scott, P. (2009). The chemical composition of the sun. *Annual Review of Astronomy and Astrophysics*, 47(1):481–522.

[Beers et al., 1994] Beers, T. C., Bestman, W., and Wilhelm, R. (1994). Emission-line candidates from the northern HK survey. , 108:268–270.

[Bromage et al., 1992] Bromage, G. E., Kellett, B. J., Jeffries, R. D., Innis, J. L., Matthews, L., Anders, G. J., and Coates, D. W. (1992). Speedy Mic: A Young; Nearby; Extremely Fast Rotating K Star Discovered by the ROSAT/WFC EUV Survey. In Giampapa, M. S. and Bookbinder, J. A., editors, *Cool Stars, Stellar Systems, and the Sun*, volume 26 of *Astronomical Society of the Pacific Conference Series*, page 80.

[Chevalier and Ilovaisky, 1997] Chevalier, C. and Ilovaisky, S. A. (1997). The ROSAT bright source RX J0222.4+4729: an active nearby short-period binary of the BY Draconis type. , 326:228–236.

[Cutispoto et al., 1997] Cutispoto, G., Kurster, M., Pagano, I., and Rodono, M. (1997). UBV(RI)c Photometry of the Rapidly Rotating K-Type Star HD197890 = "Speedy Mic". *Information Bulletin on Variable Stars*, 4419.

[Gaia Collaboration and Brown et al., 020b] Gaia Collaboration and Brown et al., A. G. A. (2020b). Gaia Early Data Release 3. Summary of the contents and survey properties.

[Gaia Collaboration and Prusti et al., 2016] Gaia Collaboration and Prusti et al., T. (2016). The Gaia mission. , 595:A1.

[Gaia Collaboration and Brown et al., 2018] Gaia Collaboration and Brown et al., A. G. A. (2018). Gaia Data Release 2. Summary of the contents and survey properties. , 616:A1.

[Guirado et al., 2011] Guirado, J. C., Marcaide, J. M., Martí-Vidal, I., Le Bouquin, J.-B., Close, L. M., Cotton, W. D., and Montalbán, J. (2011). The size of AB Doradus A from VLTI/AMBER interferometry. , 533:A106.

[Jao et al., 2003] Jao, W.-C., Henry, T. J., Subasavage, J. P., Bean, J. L., Costa, E., Ianna, P. A., and Méndez, R. A. (2003). The Solar Neighborhood. VII. Discovery and Characterization of Nearby Multiples in the CTIO Parallax Investigation. , 125:332–342.

[Kürster, 1994] Kürster, M. (1994). ROSAT observations of long-duration stellar flares. In Klare, G., editor, *Astronomische Gesellschaft Abstract Series*, volume 10 of *Astronomische Gesellschaft Abstract Series*, page 22.

[Mason et al., 2001] Mason, B. D., Wycoff, G. L., Hartkopf, W. I., Douglass, G. G., and Worley, C. E. (2001). The 2001 US Naval Observatory Double Star CD-ROM. I. The Washington Double Star Catalog. , 122:3466–3471.

[Mohanty and Basri, 2003] Mohanty, S. and Basri, G. (2003). Rotation and Activity in Mid-M to L Field Dwarfs. , 583:451–472.

[Morrissey, 2005] Morrissey, P. (2005). The on-orbit performance of the galaxy evolution explorer. *The Astrophysical Journal*, 619(1):L7–L10.

[Morrissey, 2007] Morrissey, P. (2007). The calibration and data products of GALEX. *The Astrophysical Journal Supplement Series*, 173(2):682–697.

[Osten et al., 2016] Osten, R. A., Kowalski, A., Drake, S. A., Krimm, H., Page, K., Gazeas, K., Kennea, J., Oates, S., Page, M., de Miguel, E., Novák, R., Apeltauer, T., and Gehrels, N. (2016). A Very Bright, Very Hot, and Very Long Flaring Event from the M Dwarf Binary System DG CVn. , 832:174.

[Pounds et al., 1993] Pounds, K. A., Allan, D. J., Barber, C., Barstow, M. A., Bertram, D., Branduardi-Raymont, G., Brebner, G. E. C., Buckley, D., Bromage, G. E., Cole, R. E.,

Courtier, M., Cruise, A. M., Culhane, J. L., Denby, M., Donoghue, D. O., Dunford, E., Georgantopoulos, I., Goodall, C. V., Gondhalekar, P. M., Gourlay, J. A., Harris, A. W., Hassall, B. J. M., Hellier, C., Hodgkin, S., Jeffries, R. D., Kellett, B. J., Kent, B. J., Lieu, R., Lloyd, C., McGale, P., Mason, K. O., Matthews, L., Mittaz, J. P. D., Page, C. G., Pankiewicz, G. S., Pike, C. D., Ponman, T. J., Puchnarewicz, E. M., Pye, J. P., Quenby, J. J., Ricketts, M. J., Rosen, S. R., Sansom, A. E., Sembay, S., Sidher, S., Sims, M. R., Stewart, B. C., Sumner, T. J., Vallance, R. J., Watson, M. G., Warwick, R. S., Wells, A. A., Willingale, R., Willmore, A. P., Willoughby, G. A., and Wonnacott, D. (1993). The ROSAT Wide Field Camera all-sky survey of extreme-ultraviolet sources. I - The Bright Source Catalogue. , 260:77–102.

[Singh et al., 1999] Singh, K. P., Drake, S. A., Gotthelf, E. V., and White, N. E. (1999). X-ray spectroscopy of rapidly rotating, late-type dwarf stars. *The Astrophysical Journal*, 512(2):874–891.

[Singh et al., 2014] Singh, K. P., Tandon, S. N., Agrawal, P. C., Antia, H. M., Manchanda, R. K., Yadav, J. S., Seetha, S., Ramadevi, M. C., Rao, A. R., Bhattacharya, D., Paul, B., Sreekumar, P., Bhattacharyya, S., Stewart, G. C., Hutchings, J., Annapurni, S. A., Ghosh, S. K., Murthy, J., Pati, A., Rao, N. K., Stalin, C. S., Girish, V., Sankarasubramanian, K., Vadawale, S., Bhalerao, V. B., Dewangan, G. C., Dedhia, D. K., Hingar, M. K., Katoch, T. B., Kothare, A. T., Mirza, I., Mukerjee, K., Shah, H., Shah, P., Mohan, R., Sangal, A. K., Nagabhusana, S., Sriram, S., Malkar, J. P., Sreekumar, S., Abbey, A. F., Hansford, G. M., Beardmore, A. P., Sharma, M. R., Murthy, S., Kulkarni, R., Meena, G., Babu, V. C., and Postma, J. (2014). ASTROSAT mission. In *Space Telescopes and Instrumentation 2014: Ultraviolet to Gamma Ray*, volume 9144 of , page 91441S.

[Singh et. al., 2017] Singh et. al., K. P. (2017). Soft x-ray focusing telescope aboard astrosat: Design, characteristics and performance. *Journal of Astrophysics and Astronomy*, 38(2):29.

[Stepien, 1994] Stepien, K. (1994). Applicability of the Rossby number in activity-rotation relations for dwarfs and giants. , 292:191–207.

[Tandon et al., 2020] Tandon, S. N., Postma, J., Joseph, P., Devaraj, A., Subramaniam, A., Barve, I. V., George, K., Ghosh, S. K., Girish, V., Hutchings, J. B., Kamath, P. U.,

Kathiravan, S., Kumar, A., Lancelot, J. P., Leahy, D., Mahesh, P. K., Mohan, R., Nagabhushana, S., Pati, A. K., Rao, N. K., Sankarasubramanian, K., Sriram, S., and Stalin, C. S. (2020). Additional calibration of the ultraviolet imaging telescope on board AstroSat. *The Astronomical Journal*, 159(4):158.

[Vida et al., 2009] Vida, K., Oláh, K., Kővári, Z., Korhonen, H., Bartus, J., Hurta, Z., and Posztobányi, K. (2009). Photospheric and chromospheric activity in V405 Andromedae. An M dwarf binary with components on the two sides of the full convection limit. , 504:1021–1029.

[Voges et al., 1996] Voges, W., Aschenbach, B., Boller, T., Brauninger, H., Briel, U., Burkert, W., Dennerl, K., Englhauser, J., Gruber, R., Haberl, F., Hartner, G., Hasinger, G., Kurster, M., Pfeffermann, E., Pietsch, W., Predehl, P., Rosso, C., Schmitt, J. H. M. M., Trumper, J., and Zimmermann, H.-U. (1996). ROSAT All-Sky Survey Bright Source Catalogue. , 6420.

[Voges et al., 1999] Voges, W., Aschenbach, B., Boller, T., Bräuninger, H., Briel, U., Burkert, W., Dennerl, K., Englhauser, J., Gruber, R., Haberl, F., Hartner, G., Hasinger, G., Kürster, M., Pfeffermann, E., Pietsch, W., Predehl, P., Rosso, C., Schmitt, J. H. M. M., Trümper, J., and Zimmermann, H. U. (1999). The ROSAT all-sky survey bright source catalogue. , 349:389–405.

[Wolter, U. et al., 2005] Wolter, U., Schmitt, J. H. M. M., and van Wyk, F. (2005). Doppler imaging of speedy mic using the vlt - fast spot evolution on a young k-dwarf star. *A&A*, 435(1):261–273.